Monika Ojekhile, Robert Höppner, Henning Moritz and Ludwig Mathey*

Sudden and Slow Quenches into the Antiferromagnetic Phase of Ultracold Fermions

DOI 10.1515/zna-2016-0313
Received August 23, 2016; accepted September 26, 2016; previously published online November 2, 2016

Abstract: We propose a method to reach the antiferromagnetic state of two-dimensional Fermi gases trapped in optical lattices: Independent subsystems are prepared in suitable initial states and then connected by a sudden or slow quench of the tunneling between the subsystems. Examples of suitable low-entropy subsystems are double wells or plaquettes, which can be experimentally realised in Mott insulating shells using optical super-lattices. We estimate the effective temperature T^* of the system after the quench by calculating the distribution of excitations created using the spin wave approximation in a Heisenberg model. We investigate the effect of an initial staggered magnetic field and find that for an optimal polarisation of the initial state the effective temperature can be significantly reduced from $T^* \approx 1.7\ T_c$ at zero polarisation to $T^* < 0.65\ T_c$, where T_c is the crossover temperature to the antiferromagnetic state. The temperature can be further reduced using a finite quench time. We also show that T^* decreases logarithmically with the linear size of the subsystem.

Keywords: Antiferromagnetism; Heisenberg Spins; Sudden Quench.

PACS Numbers: 67.85.-d; 71.10.Fd; 75.30.Ds.

1 Introduction

Ultracold fermions trapped in optical lattices have emerged as ideal model systems to simulate the Hubbard model [1, 2]. Major achievements include the observation of Mott insulating states [3, 4] and short-range antiferromagnetic (AF) ordering [5] and the simulation thereof [6]. Currently, the observation of long-range AF ordering is the next milestone on the quest to simulate low-temperature phases of the Hubbard model and find answers to open questions such as the origin of high-temperature superconductivity. The main experimental challenge is the reduction of entropy or temperature by at least a factor of two or four, respectively [7].

To achieve this temperature reduction, one can take advantage of the excellent tunability of ultracold atomic systems: Several cooling schemes have been proposed, which should allow to reduce the entropy of the systems (for a review, see [8]). In the scheme proposed here, we make use of the fact that in trapped systems, gapped states can be in thermal contact with gapless states, similarly as in related proposals [9–15]. As a result, the entropy in the gapped region is strongly reduced and the excitations in the gapless region carry most of the entropy. A prominent example is a band insulating state surrounded by a compressible metallic state.

We propose to transform the central band insulating shell into an AF state by first assembling subsystems featuring precursors of magnetic ordering, followed by a sudden or slow quench connecting the previously independent subsystems. We calculate the effective temperature T^* after the quench and compare it with the critical temperature for AF ordering T_c. The following questions then arise naturally: What is the ideal inital state that minimises T^*?

How does T^* depend on the size of the initial state and on the speed of the quench?

To answer the first question, we consider a double well as the simplest nontrivial subsystem, see Figure 1. An array of double wells can be created in a dimerised lattice [5, 16, 17], starting from a band insulating state and separating the sites employing, e.g. a frequency-doubled optical lattice [17]. In our limit of strong onsite interaction U, the atoms are treated as Heisenberg spins with very weak interdimer interactions J_b and strong intradimer coupling J_a. Naively, one might think that the ideal choice for the initial state of the subsystem would be a singlet state $|\psi\rangle = c_1|\uparrow\downarrow\rangle + c_2|\downarrow\uparrow\rangle$ with $|c_{1,2}|^2 = 1/2$, as this is the ground-state. However, this state has zero staggered magnetisation and hence only a small overlap to the $T = 0$ AF state.

***Corresponding author: Ludwig Mathey,** Zentrum für Optische Quantentechnologien and Institut für Laserphysik, Universität Hamburg, 22761 Hamburg, Germany,
E-mail: ludwig.mathey@physik.uni-hamburg.de
Monika Ojekhile and Robert Höppner: Zentrum für Optische Quantentechnologien and Institut für Laserphysik, Universität Hamburg, 22761 Hamburg, Germany.
http://orcid.org/0000-0001-8072-3599 (R. Höppner)
Henning Moritz: Institut für Laserphysik, Universität Hamburg, 22761 Hamburg, Germany

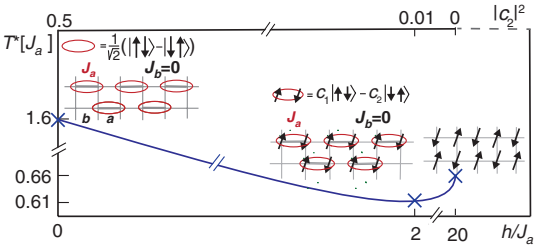

Figure 1: The effective temperature T^* after the sudden quench as a function of the initial state's coefficient c_2 or the magnetic field h. Arrows represent spins, each red ellipse denotes a singlet state $(|\uparrow\downarrow\rangle - |\downarrow\uparrow\rangle)/\sqrt{2}$ and ellipses surrounding arrows denote optimally polarised singlet states $0.99|\uparrow\downarrow\rangle - 0.12|\downarrow\uparrow\rangle$. J_a (bold) and J_b (thin lines) are the intra- and interdimer interactions.

At the other extreme, a classical Néel state with $|c_2| = 0$ already contains a preferred direction of broken symmetry and staggered magnetism. The drawback here is the perfect ordering, which is not present in larger systems even at $T = 0$ due to quantum fluctuations. The optimal state is a partially polarised state, with $|c_2/c_1| \approx 8$, featuring $T^* \approx 0.61 J_a$.

In the two-dimensional systems at finite temperature considered here, only short-range order with exponentially decaying correlations at finite temperature exists. The correlation length $\xi(T) = A \exp(2\pi\rho_s/k_B T)$ diverges exponentially for $T \to 0$. Here, $\rho_S = 0.199$ is the renormalised spin-stiffness constant at $T = 0$ and $A \approx 0.276$ [18–20]. However, the regime for which the correlation length $\xi(T)$ is larger than the lattice spacing d is referred to as the AF regime. The crossover temperature $T_c \approx 0.97 J$ is defined as $\xi(T_c) = d$. As we show below, the optimal initial state of a product state of subsystems of size L resembles the finite-temperature state in the following way: The optimal state of the subsystems also has to have a nonzero magnetisation, in analogy to the short-range order of the second-order phase transition, and the optimal temperature T^* approximately fulfills $\xi(T^*) \approx L$. The initial state therefore consists of "patches" of short-range order of length L, in analogy to the short-range ordered AF state with a correlation length $\xi(T)$. This implies that even when increasingly larger magnetically ordered subsystems with corresponding correlation lengths ξ^* are prepared, the effective temperature T^* obtained after the quench only decreases logarithmically with ξ^*, as we show numerically. We note that the correlation length $\xi(T)$ is experimentally visible in the broadening of the structure factor peaks that are obtained via Bragg scattering, in addition to technical broadening.

Our scheme has two major advantages over related schemes: Firstly, no significant redistribution of atoms is required [10, 11]. Such a redistribution is expected to cause severe problems due to the extremely slow mass flow in the Mott insulating regime [21]. Secondly, the high entropy shell surrounding the central region of interest does not necessarily have to be removed: In this case, the timescale of the quench and the subsequent thermalisation must be shorter than the time for the entropy to leak back into the central region. This condition will limit the correlation length but at the same time avoid the need for a removal step [10], which is technically very challenging and has not yet been demonstrated experimentally. All ingredients necessary for the implementation of this proposal have already been experimentally demonstrated [5, 16, 17]. Merging plaquettes to create a state of fermionic pairs has been discussed in [22]. Our scheme is closely related to the work by Lubasch and coworkers [12], where only double-well subsystems initialised in singlet states are considered.

Throughout this article, we consider fermions in the strongly repulsive coupling regime $U \gg t$, where t is the tunneling matrix element. The system is hence well described by the two-dimensional Heisenberg spin Hamiltonian

$$H = J_a \sum_{\langle ij\rangle_a} \mathbf{S}_i \mathbf{S}_j + J_b \sum_{\langle ij\rangle_b} \mathbf{S}_i \mathbf{S}_j - \sum_i h_i S_i^z, \tag{1}$$

where $\langle ij\rangle_{a/b}$ means summation over nearest neighbours along bonds a and b, respectively, and $\mathbf{S}_i$ is the spin-1/2 operator. We set $\hbar \equiv 1$ and $k_B \equiv 1$. The exchange couplings $J_{a/b} = 4t_{a/b}^2/U > 0$ quantify interactions J_a between spins in a subsystem and interactions J_b between subsystems. $t_{a/b}$ are the tunneling energies within/between subsystems. $h_i = (-1)^i h$ denotes the staggered magnetic field pointing along the z-axis. We focus on staggered magnetic fields with a spatially constant amplitude h but also touch briefly on the case with a spatially inhomogeneous amplitude in Section 4.1. Changing the ratio $g \equiv J_b/J_a$, the system undergoes a second-order phase transition. For columnar and for staggered dimerisation, it occurs at $g_c = 0.38$ [23] and $g_c = 0.396$ [24], respectively. For $g > g_c$, the groundstate has Néel order, and for $T < T_c$, the system is in the so-called renormalised classical regime. For $g < g_c$ and for $T < \Delta$, the system in the quantum disordered region with a paramagnetic ground state [18, 23], where Δ is the energy gap of the state.

We perform calculations for different initial subsystems such as double wells, 2×2 plaquettes, Z-shaped and larger $n \times m$ subsystems, see Figure 2b. The subsystems are always prepared in the groundstate of (1) with $J_b = 0$. To estimate the effective temperature, we assume that only low-energy modes are excited during the slow quench. Using linear spin-wave theory [25], we analytically (numerically)

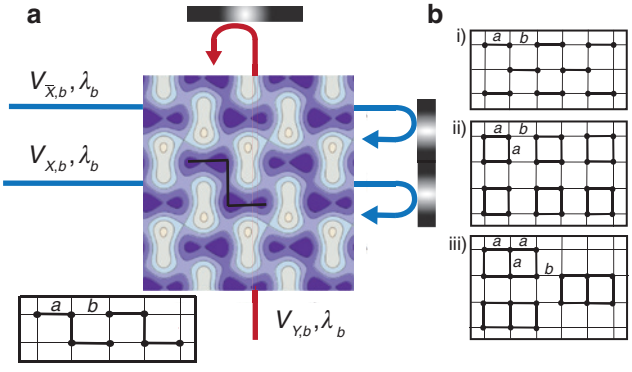

Figure 2: (a) Contour plot of the Z-shape optical lattice. Beams $\bar{X}$, X propagate along the same axis and beam Y along an axis perpendicular to that axis. Beam Y interferes with beam X. Lighter regions correspond to higher potential energy and darker to lower energy. We choose $V_{\bar{X},b} = V_{Y,b} = 1$, $V_{X,b} = 0.2$, $V_{X,r} = V_{Y,r} = 0.3$, and $\phi_1 = \pi/2$, $\phi_2 = \pi/4$. (b) Schematic pictures of dimers (i), 2×2 plaquettes (ii) and 3×2 plaquettes (iii).

estimate the temperature T^* for small (large) subsystems. We study how the effective temperature T^* depends on the quench time τ and present analytical results for slow changes.

2 Lattice Geometry

In our studies, we consider several optical lattices, simple square, and dimerised lattices as well as plaquette- and Z-shaped lattices. Dimerised and plaquette-shaped lattices have already been realised experimentally using super-lattices [17, 26] or a mixture of interfering and non-interfering lattices [5, 16].

Here, we describe a technique to create an array of four-site states in Z-shape configuration, see Figure 2a. This is the most complicated geometry which we still deem realisable with current experimental techniques. Due to the Z-shape, a staggered magnetic field can be created employing only a magnetic field gradient pointing along the diagonal axis. The larger $n\times m$ plaquettes depicted in Figure 2b-iii serve as theoretical constructs to discuss scaling issues.

For each lattice, the fundamental building block is a repulsive cubic optical lattice $V_{\bar{X},Y}(x, y)$ generated by two blue-detuned retro-reflected beams $\bar{X}$ and Y, as depicted in Figure 2a. The two beams have a wavelength of e.g. $\lambda_b = 532$ nm and a slight frequency offset to avoid mutual interference. In order to make effective bonds along the x-direction, an additional retro-reflected beam X along the x-direction is used, which interferes with beam Y. The resulting potential is $V_{X,Y}(x, y)$. The bonds along the y-direction are created by an attractive cubic optical lattice $V_{\lambda_r}(x, y)$ formed by two red-detuned retro-reflected beams at a wavelength $\lambda_r = 2\lambda_b$ (beams not shown in Figure 2a). The resulting trapping potential is shown in Figure 2a and given by the equation

$$\begin{aligned} V(x, y) &= V_{\bar{X},Y}(x, y) + V_{X,Y}(x, y) + V_{\lambda_r}(x, y) \\ &= + V_{\bar{X},b} \cdot \cos^2(k_b x) + V_{Y,b} \cdot \cos^2(k_b y) \\ &\quad + V_{X,b} \cdot \cos^2(k_b x + \phi_1) \\ &\quad + 2\sqrt{V_{X,b} V_{Y,b}} \cdot \cos(k_b x + \phi_1)\cos(k_b y) \\ &\quad - V_{X,r} \cdot \cos^2(k_r x) - V_{Y,r} \cdot \cos^2(k_r y + \phi_2), \end{aligned} \tag{2}$$

where $V_{\bar{X},b}$, $V_{X,b}$, $V_{Y,b}$, and $V_{X,r}$, $V_{Y,r}$ are the respective lattice depths. They are given in units of the recoil energy $E_b = h^2/2m\lambda_b^2$ for $V_{\bar{X},b}$, $V_{X,b}$, $V_{Y,b}$ and $E_r = h^2/2m\lambda_b^2$ for $V_{X,r}$, $V_{Y,r}$. m denotes the mass of a single atom.

3 Spin Wave Theory

To describe the final state after the quench and estimate T^*, we use linear spin-wave theory following Holstein and Primakoff (HP) [27], in the notation of [25]. We choose the classical Néel state along the z and $-z$ direction and define the rotated spin $\tilde{\mathbf{S}}_i \equiv (S_i^x, -S_i^y, -S_i^z)$, for sites i on one sublattice. Then the Hamiltonian reads

$$H = -|J| \sum_{\langle ij \rangle} S_i^z \tilde{S}_j^z + \frac{|J|}{2} \sum_{\langle ij \rangle} (S_i^+ \tilde{S}_j^+ + S_j^- \tilde{S}_i^-). \tag{3}$$

where we note that after the quench the spin couplings are equal, i.e., $J_a = J_b \equiv J$. We now approximate the spins by bosonic operators

$$S_i^+ = \sqrt{2S - n_i}\, a_i,\ S_i^- = a_i^\dagger \sqrt{2S - n_i},\ S_i^z = S - n_i, \tag{4}$$

and similarly for $\tilde{\mathbf{S}}_i$. The operators a_i, $a_i^\dagger$ satisfy commutation relations $[a_i, a_j^\dagger] = \delta_{ij}$, and $n_i \equiv a_i^\dagger a_i$ is the number of bosons on site i. It is limited by $2S$, with $S = 1/2$. We expand the square root in (4) as $\sqrt{1 - n_i/2S} \approx 1 - \frac{n_i}{4S} - \cdots$ and carry out the calculations to the lowest order, i.e. perform the linear spin wave approximation. This leads to an ensemble of noninteracting bosonic modes.

We first insert the linearised bosonic operators of (4) into the Hamiltonian (3) and use the Fourier transform $a_{\mathbf{k}} = \frac{1}{\sqrt{N}} \sum_i e^{-i\mathbf{k}\mathbf{r}_i} a_i$ where $\mathbf{k}$ runs over the first Brillouin

zone, $\mathbf{k} \in [-\pi/a, \pi/a)^2$, where a is the lattice constant, set to $a \equiv 1$. N is the number of lattice sites. The Hamiltonian becomes

$$H = -\frac{NzJS^2}{2} + zJS\sum_{\mathbf{k}}\left(a_{\mathbf{k}}^{\dagger}a_{\mathbf{k}} + \frac{\gamma_{\mathbf{k}}}{2}(a_{\mathbf{k}}a_{-\mathbf{k}} + a_{\mathbf{k}}^{\dagger}a_{-\mathbf{k}}^{\dagger})\right),$$

where $\gamma_{\mathbf{k}} \equiv \frac{1}{2}(\cos k_x + \cos k_y)$, and $\mathbf{k} = (k_x, k_y)$. z is the number of the nearest neighbours, $z = 2d$, and $d = 2$ is the lattice dimensionality. Then we perform a Bogoliubov transformation $a_{\mathbf{k}} = u_{\mathbf{k}}\alpha_{\mathbf{k}} - v_{\mathbf{k}}\alpha_{-\mathbf{k}}^{\dagger}$, with $u_k = \cosh\theta_k$ and $v_k = \sinh\theta_k$, where the $\alpha_{\mathbf{k}}$ are bosonic operators. To cancel anomalous terms in the Hamiltonian, we choose $\tanh 2\theta_{\mathbf{k}} = -\gamma_{\mathbf{k}}$. The Hamiltonian now has the desired diagonal form

$$H_{LSW} = -\frac{NzJS^2}{2} + \sum_{\mathbf{k}}\omega_{\mathbf{k}}\left(\alpha_{\mathbf{k}}^{\dagger}\alpha_{\mathbf{k}} + \frac{1}{2}\right), \tag{5}$$

where $\omega_{\mathbf{k}} = JSz\sqrt{1-\gamma_{\mathbf{k}}^2}$ is the spin-wave dispersion relation. Near $\mathbf{k} = \{0, 0\}$ and $\mathbf{k} = \{\pi, \pi\}$ the dispersion is linear with $\omega_{\mathbf{k}} \approx JSz|\mathbf{k}|$ and $\omega_{\mathbf{k}} \approx JSz|\mathbf{k} - (\pi, \pi)|$, respectively. These two Goldstone modes reflect the broken symmetry of the AF state. Due to the absence of a gap, the creation of excitations cannot be avoided even for a slow quench. The staggered magnetisation $M = \frac{1}{N}\sum_i (-1)^i \langle S_i^z\rangle$ for spin-1/2 in the linear spin-wave approximation is $M \approx 0.303$ [19, 25], so quantum fluctuations lead to a reduction to about 60% of the classical value. Numerical and theoretical studies of the staggered magnetisation in the infinite-lattice extrapolation for spin-1/2 Heisenberg models have found that $M \sim 0.25 - 0.4$ [19].

4 Sudden Quench

We now describe the method to determine the effective temperature T^* after the quench. In short, we calculate the momentum distribution of spin waves created in the quench using linear spin-wave theory, $\langle n_{\mathbf{k}}\rangle = \sum_{i,j} c_i^* c_j \langle i|\alpha_{\mathbf{k}}^{\dagger}\alpha_{\mathbf{k}}|j\rangle$, where the summation is over the basis states $|i\rangle$ of the subsystem, and $|\Psi\rangle \equiv \sum_i c_i |i\rangle$ is the groundstate. The average number of excitations $\langle n_{\mathbf{k}}\rangle$ as a function of k_x (and $k_y = 0$) for various geometries is plotted in Figure 3. The energy of the system, compared to the groundstate, after the quench is given by $\langle E\rangle = \sum_{\mathbf{k}}\langle n_{\mathbf{k}}\rangle\omega_k$. Since the system is isolated, the energy after the quench is conserved. The effective temperature T^* is then defined to be the temperature of a thermal distribution having the same energy $\langle E^{th}(T^*)\rangle = \sum_{\mathbf{k}}\langle n_{\mathbf{k}}^{th}(T^*)\rangle\omega_k$.

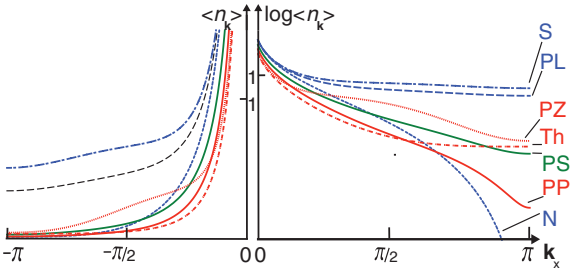

Figure 3: The average number of excitations $\langle n_{\mathbf{k}}\rangle$ on a linear and logarithmic scale as a function of k_x, for $k_y = 0$. The initial states are Néel (N), singlet (S), polarised singlet (PS), plaquette (PL), polarised plaquette (PP), polarised Z-state (PZ), and a thermal distribution (Th) with $T = 0.554\,J$. For the polarised cases, the optimal magnetic field yielding the lowest effective temperature was chosen.

An alternative measure for the temperature scale T_k^* can be defined by finding the thermal distribution $\langle n_{\mathbf{k}}^{th}(T_k^*)\rangle$ that matches the postquench distribution $\langle n_{\mathbf{k}}\rangle$ at small momenta, yielding $T_k^* = \lim_{k\to 0}\langle n_{\mathbf{k}}\rangle\omega_k$. We note that this limit is well defined because for the cases we discuss here, the limit is independent of how $\mathbf{k}$ approaches zero. We use the former definition T^*, since it takes into account not only low energy but rather all excitations created. We note that T_k^* appears when we consider slow quenches in Section VI.

4.1 Homogeneous Magnetic Field

The precise protocol of the quench is as follows: Initially, we assume that the coupling between subsystems is $J_b = 0$, and the amplitude of the staggered magnetic field h can chosen freely. The quench is initiated by suddenly increasing the coupling between subsystems, i.e. setting $J_b = J_a$. At the same time, the magnetic field is turned off. The groundstate before the quench $|\Psi\rangle$ is found by solving the Heisenberg Hamiltonian in (1) in linear spin wave approximation, see (5). The momentum distribution is determined by evaluating $\langle\Psi|\alpha_{\mathbf{k}}^{\dagger}\alpha_{\mathbf{k}}|\Psi\rangle$. We perform analytical calculations for the Néel state, singlet state, 2×2 plaquette, and Z-shape state. Details of the calculations are presented in the Appendix. For the larger $n\times m$ plaquettes, we carry out numerical calculations using exact diagonalisation. Table 1 summarises the effective temperatures found for the different configurations. We observe that with the proposed scheme the regime of AF correlations can be easily reached, with e.g. $T^* \approx 0.63\,T_c$ for optimally polarised singlets. There is good agreement between the two effective temperatures for optimally polarised states, which minimise high-energy excitations.

Table 1: The minimal energy $\langle E\rangle$ and the minimal temperatures T^* and T_k^* at optimal polarisation. For effective temperatures $T^* < T_c = 0.97\,J$ [18–20], antiferromagnetic ordering is expected.

Initial state	$\langle E\rangle$	$T^*\,[J]$	$T_k^*\,[J]$
Neel	0.158	0.66	1
Singlet	0.908	1.67	1
Polarised singlet	0.127	0.611	0.581
2×2 plaquette	0.825	1.5	1
Polarised 2×2 plaquette	0.097	0.554	0.518
Polarised Z-configuration	0.113	0.558	0.518
Polarised 4×4 plaquette	0.070	0.495	–
Polarised 5×4 plaquette	0.068	0.488	–

The much larger discrepancy for unpolarised states stems from the fact that only the low energy part of the distribution is used to determine T_k^*.

Figure 4 depicts numerical results for systems up to 20 spins in a 5×4 configuration. As the magnetic field increases, the effective temperature of the system decreases up to the minimum value T^*. After exceeding the optimal value of the magnetic field, all curves tend toward the temperature of the classical Néel state $T^* \approx 0.66\,J$. The plot shows that the magnetisation and the effective temperature go to zero with increasing size of the subsystem. We find that T^* depends weakly on the subsystem size, possibly indicating logarithmic scaling.

The explanation of this behaviour lies in the dependence of the correlation length on the temperature $\xi(T^*)$.

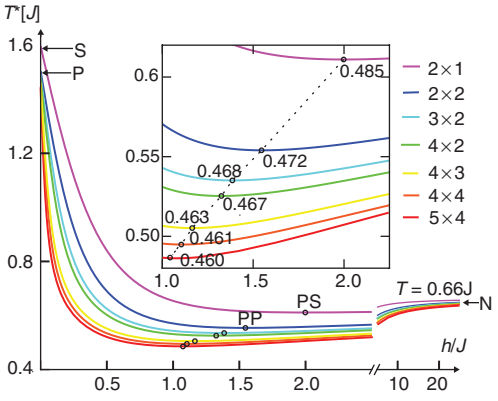

Figure 4: The effective temperature T^* as a function of the magnetic field for larger plaquette subsystems consisting of $m \times n$ sites. The inset shows the regime of $h/J_a \in [1.0 - 2.5]$. The circles mark the minimal effective temperature for each lattice geometry and the labels indicate the corresponding staggered magnetisation $M = \frac{1}{N}\sum_i \langle S_i^z\rangle$. It should approach the groundstate value $M \approx 0.303$ of the linear spin-wave approximation as the system size goes to infinity. The dotted line is a guide to the eye. The configuration labels conform to the nomenclature in Figure 3.

Inverting this formula and assuming that the correlation length is comparable to the linear size of a subsystem yields $T^* = \frac{2\pi\rho_S}{\log(L/A)}$, where we choose $L = \sqrt{m \cdot n}$ as the length scale of the subsystem. The curve is plotted in Figure 5a and compared to our numerical results (dots). We note that a 2×2 plaquette and the Z-system give almost the same energy T^*. This is consistent with the hypothesis that T^* scales only with the linear system size L.

4.2 Inhomogeneous Magnetic Field

So far, we only treated the polarisation of the initial state by a staggered magnetic field of constant amplitude h. Now we take into account a site-dependent staggered magnetic field. We consider only the case of a 4×4 plaquette. The magnetic field on each plaquette is distributed in the way shown in Figure 5b, with alternating polarity on adjacent sites. The total energy $\langle E\rangle$ is minimised by varying the three parameters h_1, h_2, and h_3. We find that the lowest energy corresponds to the case where the outer sites of the plaquette are subjected to a higher magnetic field than those in the center. The energy reaches its minimum value T_{inh}^* for $h_1/J = 1$, $h_2/J = 0.7$, $h_3/J = 0.45$. However, the reduction in effective temperature with respect to the 4×4 plaquette in a homogeneous staggered field by only $0.003\,J$ to $T_{inh}^* = 0.492\,J$ is rather small.

5 Slow Quench

In this section, we discuss the effect of a finite quench time τ on the effective temperature. We consider Néel, singlet, optimally polarised singlet states and optimally polarised 2×2 plaquettes in a homogeneous staggered magnetic field. The system is prepared in the same way as

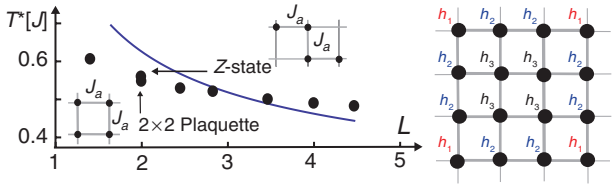

Figure 5: (a) The minimal temperature T^* as a function of the linear size of subsystems L. There is reasonable agreement between the numerical results (dots) with the expected logarithmic scaling (continuous line) expected from theory with $\rho_S = 0.199$ and $A = 0.276$ [20]. (b) Distribution of inhomogenous staggered magnetic fields over a 4×4 plaquette, the field values h_1, h_2, h_3 characterise the distribution.

in the sudden quench, but the interaction J_b between subsystems is turned on within a time interval τ, and the magnetic field h is turned off smoothly on the same timescale. To estimate the effective temperature, we make the simplifying assumption that modes with frequency $\omega_{\mathbf{k}} > 1/\tau$ adapt adiabatically to the parameter changes, whereas modes with $\omega_{\mathbf{k}} < 1/\tau$ are populated as in a sudden quench. The total energy after the quench can then be calculated as $\langle E(\tau)\rangle = \sum_{\mathbf{k}} \omega_k \langle n_k\rangle \Theta(\omega_{\mathbf{k}} - 1/\tau)$. As before, we find T^* by finding the thermal distribution having an energy $\langle E(\tau)\rangle$. As shown in Figure 6, the effective temperature drops rapidly with increasing quench time. Moreover, the effective temperatures for Néel and singlet case approach each other since their excitation densities at small momenta approach the same value.

It is instructive to find the scaling of the effective temperature with quench time in the limit of slow quenches. As it turns out, the effective temperature T^* is related to the temperature scale T_k^* associated with the low-frequency excitations and the sweep time according to $T^* \propto \left(\frac{T_k^*}{\tau^2}\right)^{1/3}$. To show this, we consider the limit in which only modes with $\mathbf{k} \approx 0$ are occupied, which have a linear dispersion $\omega_{\mathbf{k}} \sim |\mathbf{k}|$ and consequently an excitation probability $\langle n_{\mathbf{k}}\rangle \approx T_k^*/\omega_{\mathbf{k}}$. This gives the following dependence of the total energy on τ:

$$\langle E^{ad}(\tau)\rangle = \frac{1}{(2\pi)^2} \int_{\omega_{\mathbf{k}<1/\tau}} d^2\mathbf{k}\omega_k \langle n_{\mathbf{k}}\rangle = \frac{1}{4\pi}\frac{T_k^*}{\tau^2}. \tag{6}$$

We can compare this energy to the thermal energy for small temperatures:

$$\langle E^{th}_{T\to 0}\rangle = \frac{1}{(2\pi)^2} \int_0^{\mathbf{k}_{cut}} d^2\mathbf{k}\omega_k \langle n^{th}_{\mathbf{k}}\rangle = \zeta(3)\frac{T^{*3}}{\pi}, \tag{7}$$

where we again use that for $k \to 0$ the spin wave spectrum is linear and $\zeta(3) \approx 1.2$ is the Riemann zeta function. Equating these energies we find that for slow quenches the effective temperature changes according to $T^* = \left(\frac{1}{4\zeta(3)}\frac{T_k^*}{\tau^2}\right)^{1/3}$.

In this limit, the figure of merit to be optimised is thus T_k^*. We note that for even slower quenches, this power law behavior will eventually be controlled by the critical point at g_c. In this limit, the power-law exponent would be replaced by critical exponents.

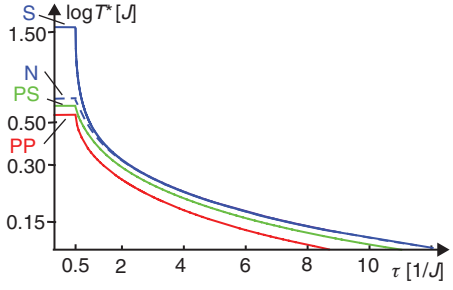

Figure 6: The effective temperature T^* as a function of the quench time τ on a log-lin scale. The different configurations are labelled as in previous figures. As τ increases, the effective temperature T^* quickly approaches power-law scaling, $T^* \sim (T_k^*/\tau^2)^{1/3}$.

6 Summary

In conclusion, we have proposed a method and a specific experimental realisation to reach the antiferromagnetically ordered state by preparing very low entropy subsystems, which do not interact initially. The subsystems are merged by either sudden or slow quenches of the interaction, where slower quenches result in significantly lower effective temperatures. The effective temperature is calculated within linear spin-wave theory, and we observe that it reduces with increasing linear subsystems size. Assuming that the subsystem size determines the correlation length of the resulting AF state, we expect logarithmic scaling. In addition, we find that the effective temperature can be reduced if the subsystems are prepared with optimal polarisation, closely resembling the target state. We expect that these insights will be very useful to attain AF ordering in experiments employing double well or plaquettes type geometries. As shown in Section 2, the method can be implemented with current technology. Furthermore, the principle that is outlined here, i.e. to assemble subsystems with precursors of the desired short-range order, can also be applied to the construction of other many-body states in ultracold atom systems.

Acknowledgments: We acknowledge support from the Deutsche Forschungsgemeinschaft through the SFB 925 and the Landesexzellenzinitiative Hamburg, which is supported by the Joachim Herz Stiftung.

Appendix

In our analytical computations, we consider the following states:

1. Classical Néel state. This state is a product state of spins up $|\uparrow\rangle$ and spins down $|\downarrow\rangle$ ordered in a checkerboard $|0\rangle \equiv |\uparrow\downarrow\uparrow\downarrow\ldots\rangle$.

2. Polarised singlet state. This is a product state of singlets that are arranged as shown in picture Figure 2b i. We represent it by the formula:

$$(\prod_i (c_1 - c_2 \alpha^\dagger_{i,1}\alpha^\dagger_{i,2}))|0\rangle.$$

In the presence of nonzero h, the coefficients c_1 and c_2 are generally not equal to each other only for $h=0$, $c_1=c_2$, and the standard singlet state is recovered by putting $c_1 = 1/\sqrt{2}$.

3. Polarised 2×2 plaquette state. This is a product state of 2×2 plaquettes that are arranged as shown in picture Figure 2b ii. We represent it by the formula:

$(\prod_i (c_1 + c_2 \prod_{j=1}^4 \alpha^\dagger_{i,j} + c_3 \sum_{j=1}^4 \alpha^\dagger_{i,j}\alpha^\dagger_{i,j+1}))|0\rangle$. For $h=0$, the coefficients are following $c_1 = c_2 = -\frac{1}{\sqrt{3}}$, $c_3 = \frac{1}{2\sqrt{3}}$.

4. Polarised Z-state. This is a product state of Z-states that are arranged as shown in picture Figure 2a. We represent it by the formula:

$$(\prod_i (c_1 + c_2 \prod_{j=1}^4 \alpha^\dagger_{i,j} + c_3 \alpha^\dagger_{i,2}\alpha^\dagger_{i,3} + c_4 \alpha^\dagger_{i,1}\alpha^\dagger_{i,4} + c_5(\alpha^\dagger_{i,1}\alpha^\dagger_{i,2} + \alpha^\dagger_{i,3}\alpha^\dagger_{i,4})))|0\rangle$$

In all above-mentioned states, $|0\rangle$ is the classical Néel state, α_i, $\alpha_i^\dagger$ are the annihilation and creation bosonic quasiparticle operators at the lattice site i. They are Fourier transformed operators discussed before in the part 'spin wave theory'. All states are normalised, $\sum_i |c_i|^2 = 1$.

The momentum distributions of Bogoliubov excitations created in the sudden quench for the above states are following:

1. For Néel state,

$$\langle n_{\mathbf{k}}\rangle = \frac{1}{2\sqrt{1-\gamma_{\mathbf{k}}^2}} - \frac{1}{2}, \tag{8}$$

2. For polarised singlet state

$$\langle n_{\mathbf{k}}\rangle = \frac{c_2^2 + \frac{1}{2} - \gamma_{\mathbf{k}} c_2\sqrt{1-c_2^2}\cos k_x}{\sqrt{1-\gamma_{\mathbf{k}}^2}} - \frac{1}{2} \tag{9}$$

3. For polarised 2×2 plaquette state

$$\langle n_{\mathbf{k}}\rangle = \frac{f_1(\mathbf{c})}{2\sqrt{1-\gamma_{\mathbf{k}}^2}} - \frac{1}{2} + 2c_3^2 \sin k_x \sin k_y, \tag{10}$$

where $\mathbf{c} = (c_1, c_2, c_3)$ and

$$f_1(\mathbf{c}) = 2c_2^2 + 4c_3^2(1+\cos k_x \cos k_y) + (\cos k_x + \cos k_y)^2(c_2c_3 + c_1c_3) + 1, \tag{11}$$

4. For polarised Z-state,

$$\langle n_{\mathbf{k}}\rangle = \frac{f_2(\mathbf{c})}{2\sqrt{1-\gamma_{\mathbf{k}}^2}} - \frac{1}{2}, \tag{12}$$

where $\mathbf{c} = (c_1, \ldots, c_5)$ and $f_2(\mathbf{c}) = \sum_{i=1}^5 C_i(\mathbf{c})$

$$\begin{aligned} C_1(\mathbf{c}) &= 1 + 2(c_2^2 + c_5^2) + c_3^2 + c_4^2 \\ C_2(\mathbf{c}) &= 2(c_3 + c_4)B_5 \cos(k_x - k_y) \\ C_3(\mathbf{c}) &= 2\gamma_{\mathbf{k}}(c_1 + c_2)c_5 \cos k_x \\ C_4(\mathbf{c}) &= \gamma_{\mathbf{k}}(c_2c_3 + c_1c_5)\cos(2k_x - k_y) \\ C_5(\mathbf{c}) &= \gamma_{\mathbf{k}}(c_1c_3 + c_2c_5)\cos k_y. \end{aligned} \tag{13}$$

In all above-mentioned formulas $\gamma_{\mathbf{k}} = \frac{1}{2}(\cos k_x + \cos k_y)$.

Now we calculate the total energy after the sudden quench, $\langle E\rangle = \sum_{\mathbf{k}} \omega_{\mathbf{k}} \langle n_{\mathbf{k}}\rangle$ in all above states, $\omega_{\mathbf{k}}$ is the spin wave dispersion. Energies in the thermodynamic limit are the following:

1. For Néel state, $\langle E\rangle \approx 0.158$.
2. For polarised singlet state,

$$\langle E\rangle \approx 2c_2^2 + \frac{1}{2}c_2\sqrt{1-c_2^2} + 0.16. \tag{14}$$

3. For polarised 2×2 plaquette state,

$$\langle E\rangle \approx 2(c_2^2 + 2c_3^2) + (c_2c_3 + c_1c_3) + 0.16. \tag{15}$$

4. For polarised Z-state

$$\langle E\rangle \approx 2(c_2^2 + c_5^2) + c_3^2 + c_4^2 + \frac{1}{4}(c_1c_3 + c_2c_4 + 2c_1 + 2c_2) + 0.16. \tag{16}$$

Above energies are convex functions of c_i's so they can be optimised over the external magnetic field h. The Lagrangian multipliers are used to estimate their minima. Energies with optimal magnetic field h are compared to the energy of thermal distribution with temperature T^* in the thermodynamic limit, $\langle E^{th}\rangle = \frac{1}{4\pi^2}\int d^2\mathbf{k}\,\omega_{\mathbf{k}}\langle n_{\mathbf{k}}^{th}(T^*)\rangle$. The resulting temperature is denoted as T^*.

Now we approximate the effective temperature T^* for an adiabatic quench. In this case, we calculate the number of spin waves in the long-wavelength limit $\langle n_{k_x}\rangle \equiv \langle n_{\mathbf{k}}\rangle_{k_x\to 0}$ (we set $k_y = 0$):

1. For Néel state, $\langle n_{k_x}\rangle = \frac{1}{2\sqrt{1-\gamma_{\mathbf{k}}^2}}$.

2. For polarised singlet state, $\langle n_{k_x}\rangle = \frac{g_1(c_2)}{\sqrt{1-\gamma_{\mathbf{k}}^2}}$, where $g_1(c_2) = c_2^2 + \frac{1}{2} - c_2\sqrt{1-c_2^2}$.

3. For polarised 2×2 plaquette state, $\langle n_{k_x}\rangle = \frac{g_2(\mathbf{c})}{\sqrt{1-\gamma_k^2}}$, where $\mathbf{c} = (c_1, c_2, c_3)$ and

$$g_2(\mathbf{c}) = (c_2^2 + 2c_3^2) + 2c_3^2 + 2(c_2c_3 + c_1c_3) + \frac{1}{2}. \quad (17)$$

4. For polarised Z-state, $\langle n_{k_x}\rangle = \frac{g_3(\mathbf{c})}{\sqrt{1-\gamma_k^2}}$, where $\mathbf{c} = (c_1, \ldots, c_5)$ and

$$g_3(\mathbf{c}) = \frac{1}{2}\left(2c_2^2 + \sum_{i=3}^{5} c_i^2\right) + \frac{1}{2}((c_1 + c_2)(c_3 + c_4)) + c_5\sum_{i=1}^{4} c_i + \frac{1}{2}. \quad (18)$$

Since $g_i(\mathbf{c})$ are convex functions, there is a magnetic field that optimises $\langle n_{k_x}\rangle$. We use again the Lagrangian multipliers to find minima of $\langle n_{k_x}\rangle$. We notice that $\langle n_{k_x}\rangle$ diverges the same way as a thermal distribution for small energies $\langle n_k^{th}\rangle \approx \frac{T^*}{\omega_k}$. Comparing them we obtain the minimal temperature $T_{k_x}^*$.

References

[1] I. Bloch, J. Dalibard, and W. Zwerger, Rev. Mod. Phys. **80,** 885 (2008).
[2] T. Esslinger, Annu. Rev. Condens. Matter Phys. **1,** 129 (2010).
[3] R. Jördens, N. Strohmaier, K. Günter, H. Moritz, and T. Esslinger, Nature **455,** 204 (2008).
[4] U. Schneider, L. Hackermüller, S. Will, T. Best, I. Bloch, T. A. Costi, R. W. Helmes, D. Rasch, and A. Rosch, Science **322,** 1520 (2008).
[5] D. Greif, T. Uehlinger, G. Jotzu, L. Tarruell, and T. Esslinger, Science **340,** 1307 (2013).
[6] J. Simon, W. S. Bakr, R. Ma, M. E. Tai, P. M. Preiss, and M. Greiner, Nature **472,** 307 (2011).
[7] R. Jördens, L. Tarruell, D. Greif, T. Uehlinger, N. Strohmaier, H. Moritz, T. Esslinger, L. De Leo, C. Kollath, A. Georges, V. Scarola, L. Pollet, E. Burovski, E. Kozik, and M. Troyer, Phys. Rev. Lett. **104,** 180401 (2010).
[8] D. C. McKay and B. deMarco, Rep. Prog. Phys. **74,** 054401 (2011).
[9] B. Capogrosso-Sansone, S. G. Söyler, N. Prokof'ev, and B. Svistunov, Phys. Rev. A **77,** 015602 (2008).
[10] J.-S. Bernier, C. Kollath, A. Georges, L. De Leo, F. Gerbier, C. Salomon, and M. Köhl, Phys. Rev. A **79,** 061601 (2009).
[11] T.-L. Ho and Q. Zhou, Proc. Natl. Acad. Sci. U.S.A. **106,** 6916 (2009).
[12] M. Lubasch, V. Murg, U. Schneider, J. I. Cirac, and M.-C. Bañuls, Phys. Rev. Lett. **107,** 165301 (2011).
[13] T. Paiva, Y. L. Loh, M. Randeria, R. T. Scalettar, and N. Trivedi, Phys. Rev. Lett. **107,** 086401 (2011).
[14] C. J. M. Mathy, D. A. Huse, and R. G. Hulet, Phys. Rev. A **86,** 023606(R) (2012).
[15] M. Colomé-Tatché, C. Klempt, L. Santos, and T. Vekua, New J. Phys. **13,** 113021 (2011).
[16] M. Anderlini, P. J. Lee, B. L. Brown, J. Sebby-Strabley, W. D. Phillips, and J. V. Porto, Nature **448,** 452 (2007).
[17] S. Trotzky, P. Cheinet, S. Fölling, M. Feld, U. Schnorrberger, A. M. Rey, A. Polkovnikov, E. A. Demler, M. D. Lukin, I. Bloch, Science **319,** 295 (2008).
[18] S. Chakravarty, B. I. Halperin, and D. R. Nelson, Phys. Rev. B **39,** 2344 (1989); A. V. Chubukov, S. Sachdev, and J. Ye, Phys. Rev. B **49,** 11919 (1994).
[19] E. Manousakis, Rev. Mod. Phys. **63,** 1 (1991).
[20] H. Q. Ding and M. S. Makivić, Phys. Rev. Lett. **64,** 1449 (1990).
[21] C.-L. Hung, X. Zhang, N. Gemelke, C. Chin, Phys. Rev. Lett. **104,** 160403 (2010).
[22] A. M. Rey, R. Sensarma, S. Fölling, M. Greiner, E. Demler, and M. D. Lukin, Eur. Phys. Lett. **87,** 60001 (2009).
[23] S. Sachdev, Science **288,** 475 (2000).
[24] F.-J. Jiang, arXiv:**1307,** 6104 (2013).
[25] A. Auerbach, Interacting Electrons and Quantum Magnetism, Springer-Verlag, New York 1998.
[26] S. Nascimbène, Y. A. Chen, M. Atala, M. Aidelsburger, S. Trotzky, B. Paredes, I. Bloch, Phys. Rev. Lett. **108,** 205301 (2012).
[27] T. Holstein and H. Primakoff, Phys. Rev. **58,** 1098 (1940).